Assessment of Fin Thickness Influence on Melting and Solidification Processes Inside Longitudinally Finned Latent Thermal Energy Storage

Mateo Kirincic, Anica Trp, Kristian Lenic, Josip Batista

University of Rijeka, Faculty of Engineering, Department of Thermodynamics and Energy Engineering, Vukovarska 58, 51000 Rijeka, Croatia

Abstract

In the paper, series of numerical investigations have been performed in order to evaluate the influence of fin thickness on melting and solidification performance inside the shell-and-tube type longitudinally finned latent thermal energy storage (LTES). The LTES uses water as the heat transfer fluid (HTF) and RT 25 paraffin as the phase change material (PCM). Using experimentally validated mathematical model and numerical procedure, numerical investigations of PCM melting and solidification have been carried out for various fin thicknesses; 0.5 mm, 2 mm and 4 mm. Thermal energy stored in 8 h of charging, during which the PCM melts, and released in 12 h of discharging, during which the PCM solidifies, as well as melting and solidification rates, were compared. Time-wise variations of average liquid fractions and fin temperatures have been obtained for all configurations during melting and solidification processes. The results indicate that, due to increased fin capacity, thicker fins expedite melting/solidification rate. However, due to reduced amount of the PCM as the result of using thicker fins, less thermal energy can be stored in and released from the LTES. As indicated by the investigation, fin thickness is an influential geometry parameter which should be carefully selected in order to maximize the LTES thermal performance.

Keywords: Latent thermal energy storage, melting and solidification, fin thickness, numerical investigation.

1. Introduction

Thermal energy storage plays a crucial role in solar energy-based thermal systems. Since solar energy is only available during the day, thermal energy storage helps bridge the gap between solar energy availability and heating demand, thereby improving the efficiency of the thermal system. There are three types of thermal energy storage: sensible, latent, and thermochemical. In latent thermal energy storage (LTES) system, the heat acquired by solar collectors is transferred to a phase change material (PCM) through a heat transfer fluid (HTF) during the charging period (melting) and released during the discharging period (solidification). LTES are implemented in various fields of thermal engineering, e.g. domestic heating systems, refrigeration, solar-powered plants and processing facilities etc. However, a major downside of LTES technology is relatively low thermal conductivity of the PCMs, especially organics, which include paraffins and fatty acids, mostly used in low temperature HVAC systems. This hinders heat transfer, resulting in reduced charging/discharging power and less accumulated/released energy (Khan et al., 2016). To overcome this issue, several approaches can be adopted. Varying the LTES geometry parameters, such as increasing the LTES length/height, aspect ratios and tube diameters (Modi et al., 2023) or implementing fins results in increased heat transfer surface area and/or decreased PCM thickness (thus decreasing the PCM thermal resistance), which both increase the overall heat transfer. The PCM effective thermal conductivity can be enhanced by inserting high conductivity nanoparticles (Yu et al., 2023), foams (Fteiti et al., 2023) or matrices (Kumar and Saha, 2020) into the PCM. Due to their affordability and simplicity in design, manufacture and implementation process, the addition of fins is the most commonly used enhancement (Liu et al., 2012). A variety of fin designs has been investigated experimentally and numerically, and their geometry parameters have been optimized according to specified objectives.

Rathod and Banerjee (2015) have experimentally investigated charging and discharging performance enhancement in a shell-and-tube LTES using stearic acid as the PCM and water as the HTF. By installing three longitudinal fins, melting time has been reduced by up to 25%, while solidification time has been reduced by up to 44% in comparison to the plain tube configuration. Z. Khan and Z.A. Khan (2017) have experimentally

Selection and/or peer review under responsibility of Scientific Committee
10.18086/eurosun.2024.06.02 Available at http://proceedings.ises.org

investigated LTES thermal performance during charging in a LTES with novel type longitudinal fins. Compared to the plain tube configuration, melting time and mean charging power have been enhanced by up to 70%. The effect of using eight longitudinal fins per tube on the charging/discharging process of shell-and-tube LTES was quantitatively compared by Kirincic et al. (2021a), assessing the performance of a finned design against a configuration without fins. The implementation of fins resulted in a significant enhancement of thermal performance throughout both the charging and discharging cycles. In comparison to the finless design, the addition of fins reduced melting/solidification time by 52%/43%. To examine the overall efficiency of the LTES, comprehensive LTES efficiency was defined as the ratio of stored/released thermal energy and the maximum LTES thermal capacity for the finless design. The finned design exhibited superior performance compared to the design without fins, as the chosen fin type and parameters did not notably decrease the amount of stored/released thermal energy while substantially promoting the heat transfer rate.

Yu et al. (2020) investigated the melting behavior of RT 58 paraffin in a horizontal LTES with eight non-uniformly distributed longitudinal fins. They performed an optimization of fin angle gradient and fin thickness gradient with the objective of minimizing melting time. For the optimized LTES configuration, a decrease in total melting time by 30.5% in comparison with the uniform fin configuration was observed. Yang et al. (2017) investigated the influence of radial fins on heat transfer in a shell-and-tube LTES which uses paraffin as the PCM and water as the HTF. The influence of fin number, fin thickness and fin spacing on heat transfer was assessed and a decrease in melting time by 65% compared to the equivalent time in the finless configuration was observed. Additionally, the authors noted that increasing fin number and fin thickness beyond a specific value can have a negative effect on heat transfer, as well as LTES heat storing/releasing capacity as the influence of natural convection and the amount of the PCM are both reduced.

In this paper, influence of fin thickness on LTES thermal performance during melting and solidification processes is numerically evaluated by comparing melting/solidification rates and energies stored in 8 h of charging and released in 12 h of discharging for LTES configurations with fin thicknesses of 0.5 mm, 2 mm and 4 mm.

2. Mathematical model and numerical solving

2.1 Physical problem and computational domain

Numerical investigation has been conducted on the PCM melting and solidification in a vertically oriented shell-and-tube LTES tank. The LTES tank consists of a 950 mm diameter outer shell and has a height of 1500 mm, with 19 concentric aluminum tubes with inner and outer diameters of 25 mm and 30 mm, respectively. Water is used as the HTF and flows through the tubes, entering the tank at the top. The PCM used is technical grade paraffin (RT 25), which fills the shell-side. During the charging process (daytime), hot HTF transfers heat to the PCM, causing it to melt and accumulate heat. During the discharging process (nighttime), the PCM solidifies and releases stored heat to the cold HTF. Each tube features eight equidistant longitudinal fins installed on the PCM-side. The fins are 66 mm wide with fin investigated thicknesses of 0.5, 2 and 4 mm.

Performed experimental investigations on low temperature organic PCM indicate that the melting process is non-isothermal, occurring within a narrow temperature range, while solidification is typically isothermal at a nearly constant temperature. These distinctions have been taken into account and thermophysical properties of the PCM used in the numerical investigation, based on the manufacturer's data sheet (Rubitherm GmbH, 2018), are given in Tab. 1.

The computational domain represents the smallest segment of the analyzed physical problem and encompasses all physical phenomena within the LTES tank. In the multi-tube LTES, thermal behavior in and around geometrically identical tubes is very similar, i.e. observing the physical phenomena in and around one HTF tube is sufficiently representative of the thermal behavior of the whole LTES. Regions of influence of each tube can be defined with circles circumscribed around each of them, with the diameter of the circles being equal to the tube pitch. Therefore, it is sufficient to investigate the heat transfer process around a single tube and its PCM annulus. Due to the tube geometry and physical symmetry, the investigated region can be further simplified so that includes one-eighth of a single tube, containing the corresponding HTF segment, tube

segment, halves of adjacent fins and its surrounding PCM annulus segment. The computational domain is divided into three subdomains: the HTF subdomain, the tube wall and fins subdomain, and the PCM subdomain. In Figure 1, tube configuration inside the LTES, a single tube and its surrounding PCM annulus, as well as the selected computational domain are shown.

Tab. 1. Thermophysical properties of the PCM

Property	PCM
Melting temperature range, °C	18-25
Solidification temperature, °C	25
Specific heat capacity, J/kgK	2000
Specific latent heat, J/kg	170000
Thermal conductivity, W/mK	0.2
Density, kg/m^3	820
Dynamic viscosity, Pa·s	0.0036
Thermal expansion coefficient, 1/K	0.001

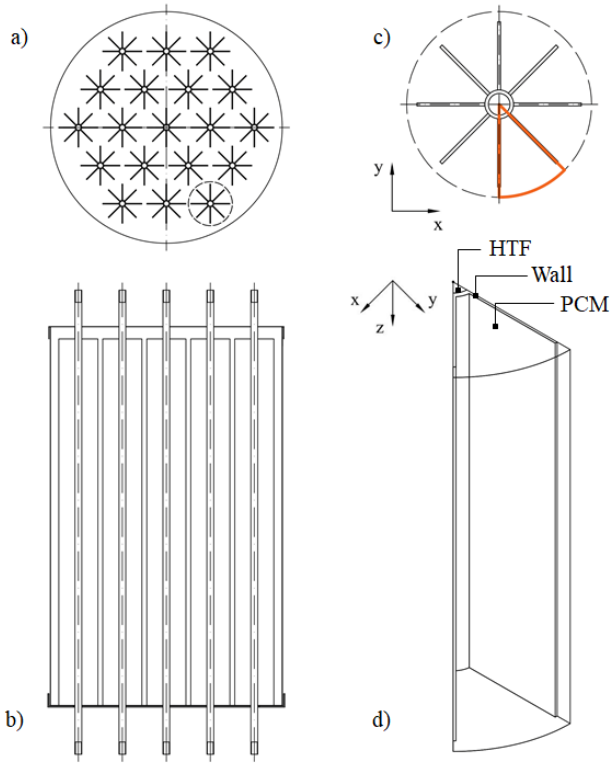

Fig. 1. Investigated LTES tank, a) top view, b) longitudinal cross-section view, c) transversal cross-section of a single finned tube with surrounding PCM annulus and denoted computational domain, d) selected computational domain in 3D view.

2.1 Governing equations, initial and boundary conditions

For the physical problem involving a transient conjugated problem that includes forced convection, conduction, and phase change heat transfer, including natural convection occurring in the liquid phase of the PCM, a 3D mathematical model has been developed. It uses the enthalpy formulation describe heat transfer during the melting and solidification of the PCM, where specific enthalpy is the calculated variable instead of temperature in the PCM energy equation. Natural convection in the liquid phase of the PCM significantly affects heat transfer during melting but has only a minor impact during solidification. Previous work by the

authors has shown that neglecting natural convection during solidification leads to a small error but significantly reduces computation time (Kirincic et al., 2021b). Therefore, in the current study, natural convection in the PCM subdomain is considered only during the melting process.

Several assumptions have been made regarding the physical properties, such as assuming constant thermophysical properties for all materials, homogeneous and isotropic PCM with equal physical properties in both solid and liquid phases, incompressible and laminar flow of the HTF and liquid PCM during melting (with both fluids considered as Newtonian). The operating conditions assume constant HTF inlet velocities and inlet temperatures, uniform initial temperature distributions throughout the computational domain for both charging and discharging analyses, and neglecting heat dissipation through the top and bottom of the LTES tank. Modeling of natural convection effects in the liquid PCM during melting has been included through the Boussinesq approximation.

The governing equations, based on these assumptions, are applied to each subdomain and are presented below. For concision, momentum equations have been condensed so that *i* represents x, y and z direction in their respective equations.

HTF

- continuity

$$\mathrm{div}\,\vec{\boldsymbol{w}} = 0 \qquad \text{(eq. 1)}$$

- momentum

$$\frac{\partial(\rho_{HTF}\cdot w_i)}{\partial t} + \mathrm{div}(\rho_{HTF}\cdot w_i\cdot\vec{\boldsymbol{w}}) = \frac{\partial p}{\partial i} + \mathrm{div}(\mu_{HTF}\cdot \mathrm{grad}\, w_i) \qquad \text{(eq. 2)}$$

- energy

$$\frac{\partial(\rho_{HTF}\cdot T)}{\partial t} + \mathrm{div}(\rho_{HTF}\cdot\vec{\boldsymbol{w}}\cdot T) = \frac{k_{HTF}}{c_{HTF}}\mathrm{div}(\mathrm{grad}\, T) \qquad \text{(eq. 3)}$$

Wall

- energy

$$div(\rho_w\cdot\vec{\boldsymbol{w}}\cdot T) = \frac{k_w}{c_w}\mathrm{div}(\mathrm{grad}\, T) \qquad \text{(eq. 4)}$$

PCM

- continuity

$$\mathrm{div}\,\vec{\boldsymbol{w}} = 0 \qquad \text{(eq. 5)}$$

- momentum

$$\frac{\partial(\rho_{PCM}\cdot w_i)}{\partial t} + \mathrm{div}(\rho_{PCM}\cdot w_i\cdot\vec{\boldsymbol{w}}) = \left(\rho_{PCM} - \rho_{0,PCM}\right)\cdot g_i - \frac{\partial p^*}{\partial i} + \mathrm{div}(\mu_{PCM}\cdot \mathrm{grad}\, w_i) + S_i \qquad \text{(eq. 6)}$$

Momentum sinks are incorporated to consider the velocity damping that occurs within the phase change region of the PCM (referred to as the "mushy zone"). The mushy zone is characterized as a porous region (Brent et al., 1988), and the formulations for the momentum sinks are based on the Carman-Kozeny equations, which describe flow through porous media:

$$S_i = \frac{(1-\gamma)^2}{\gamma^3+\varepsilon}\cdot A_{mush}\cdot w_i \qquad \text{(eq. 7)}$$

The intensity of velocity damping is dependent on A_{mush} [kg/m^{3}s], a morphological or „mushy zone" constant, which is usually a large number. In the present investigation, a value of 10^6 has been used. Dividing by zero is

prevented by including the parameter ε, a very small number, set in the expressions to 0.001. The parameter γ is the liquid fraction and it represents the porosity of a cell in the mushy zone. When the specific enthalpy in the PCM region is between H_s and H_l, liquid fraction is calculated as:

$$\gamma = \frac{H - H_s}{H_l - H_s} \quad \text{(eq. 8)}$$

H_s represents solidus specific enthalpy and has a value of $c_{PCM} \cdot T_s$ and H_l represents liquidus specific enthalpy, with the value of $c_{PCM} \cdot T_l + L$.

- energy

$$\frac{\partial(\rho_{PCM} \cdot H)}{\partial t} + \mathrm{div}(\rho_{PCM} \cdot \vec{\boldsymbol{w}} \cdot H) = \frac{k_{PCM}}{c_{PCM}} \mathrm{div}(\mathrm{grad}\, H) \quad \text{(eq. 9)}$$

Temperature is calculated from numerically obtained specific enthalpies in the following way:

$$H \leq H_s \rightarrow T = \frac{H}{c_{PCM}} \quad \text{(eq. 10)}$$

$$H_s \leq H \leq H_l \rightarrow T = T_s + (T_l - T_s) \cdot \frac{H - H_s}{c_{PCM} \cdot (T_l - T_s) + L} \quad \text{(eq. 11)}$$

$$H \geq H_l \rightarrow T = \frac{H - L}{c_{PCM}} \quad \text{(eq. 12)}$$

Equations (1)-(6) and (9) are solved when melting processes are simulated. When solidification processes are considered, governing equations regarding the PCM subdomain are reduced to the energy equation, describing conductive heat transfer:

$$\frac{\partial(\rho_{PCM} \cdot H)}{\partial t} = \frac{k_{PCM}}{c_{PCM}} \mathrm{div}(\mathrm{grad}\, H) \quad \text{(eq. 13)}$$

Equations (1)-(4) remain unchanged when solidification processes are investigated since they are governing equations for the HTF and wall subdomains.

In the initial moment, uniform temperature distribution throughout the computational domain is defined, below the solidus temperature in melting simulations and above solidification temperature in solidification simulations. Also, the HTF is assumed to be stationary, i.e. its velocity has been set to zero. It can be written:

$$T = T_{init};\ w_x = 0;\ w_y = 0;\ w_z = 0 \quad \text{(eq. 14)}$$

Boundary conditions are defined at the outer boundaries of the computational domain and at the boundaries between subdomains. The inlet boundary condition is specified at the HTF inlet, providing the inlet temperature and velocity values. The outlet boundary condition assumes fully developed fluid flow, where there is no variation in variables in the flow direction, and is applied at the HTF outlet.

At the top and bottom regions of the PCM and wall, adiabatic boundary conditions are applied, considering them to be perfectly insulated. In the fluid PCM subdomain (in melting simulations), the no-slip condition is also applied at these boundaries, indicating that the fluid velocity at the boundary is zero. Heat transfer by conduction is defined in the thin layer along the boundaries between the HTF and the wall, as well as between the PCM and the wall. Furthermore, at those boundaries, the no-slip condition is also applied in the HTF subdomain, as well as in the PCM subdomain in melting simulations. For the outer domain boundaries in the HTF, wall and PCM subdomains, symmetry boundary conditions are defined, assuming that the flow and temperature profiles are symmetrical with respect to these boundaries. A schematic of the boundary conditions has been provided in Fig. 2. In Fig. 2, asterisks (*) denote that the expression is only applied when natural convection is considered, i.e. in melting investigations.

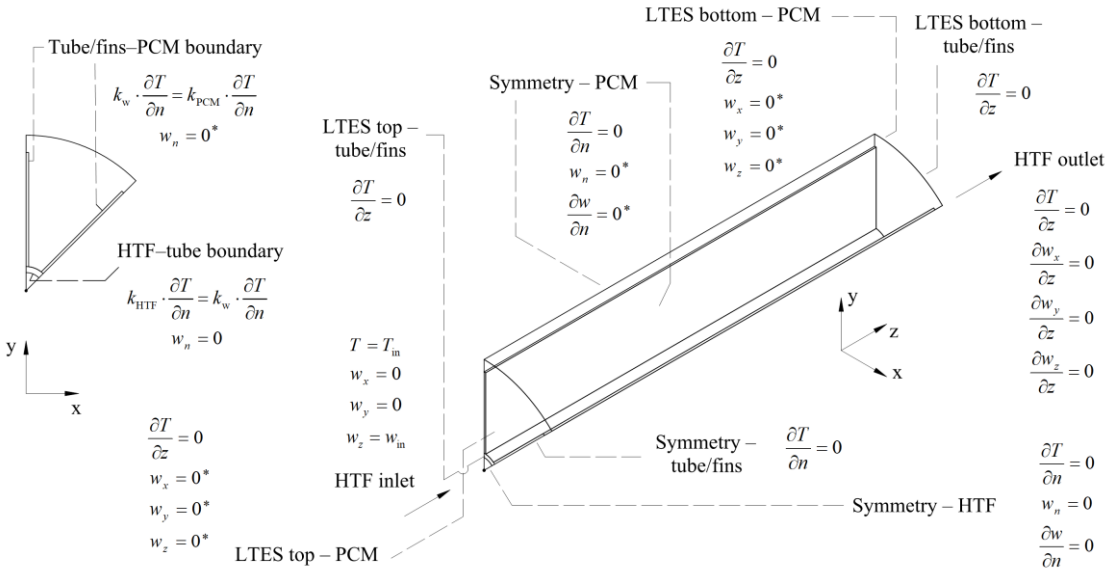

Fig. 2. Boundary conditions schematic in the xy plane and in 3D view

2.2 Numerical procedure

Numerical solution has been obtained by ANSYS Fluent numerical solver that uses the finite volume method (Versteeg and Malalasekera, 1995). Pressure and velocity fields have been coupled using the SIMPLE algorithm. Pressure Staggering Option scheme (PRESTO!) has been used to discretize pressure correction equations. Quadratic upwind scheme (QUICK) has been used to discretize convective terms in momentum and energy equations. Fully implicit discretization in time has been implemented. Under-relaxation factors of 0.3, 0.6 and 1 have been used for pressure, momentum and energy equations, respectively. Convergence criteria of 10^{-3} for continuity and 10^{-6} for momentum and energy equations have been used.

Temperature was coupled with specific enthalpy at the boundaries between the wall (tube and fins) and the PCM subdomains using a series of self-written user-defined functions (UDFs). Momentum sinks, as described in eq. (7), and the conversion of specific enthalpy to temperature according to eqs. (10)-(12) were implemented into the numerical procedure using UDFs. Mesh and timestep independence studies were previously performed (Kirincic et al., 2024a,b) and appropriate mesh size (268500 cells) and timestep (0.1 s) have been selected.

3. Experimental validation

Validation of the mathematical model and numerical procedure was performed through experimental measurements conducted on the constructed LTES tank with the specified geometry characteristics and fin thickness of 2 mm. The LTES tank used Rubitherm's RT 25 paraffin as the PCM and water as the HTF. To prevent heat dissipation to the surroundings, the tank was insulated with expanded rubber foam. The experimental measurements took place at the Laboratory for Thermal Measurements at the University of Rijeka, Faculty of Engineering.

The experimental setup consisted of a shell-and-tube LTES tank, water-water heat pump with hot and cold water supply tanks, a control valve, circulation pumps, temperature sensors, flow meters, and an automatic control system to maintain a constant water temperature at the LTES inlet. A full description of the experimental system can be found in Kirincic et al. (2021c). Temperature measuring was performed using thermocouples, with measurement uncertainty of 0.37 °C (Kirincic, 2021), placed at specific positions around selected tubes on the PCM-side of the tank, as well as at the water inlet and outlet. Measured temperatures were recorded and stored into computer memory at 10-second intervals through a LabView application, which received and processed data from the data acquisition unit. Parts of the experimental setup, as well as the positions of thermocouples around a single examined tube are shown in Fig. 3.

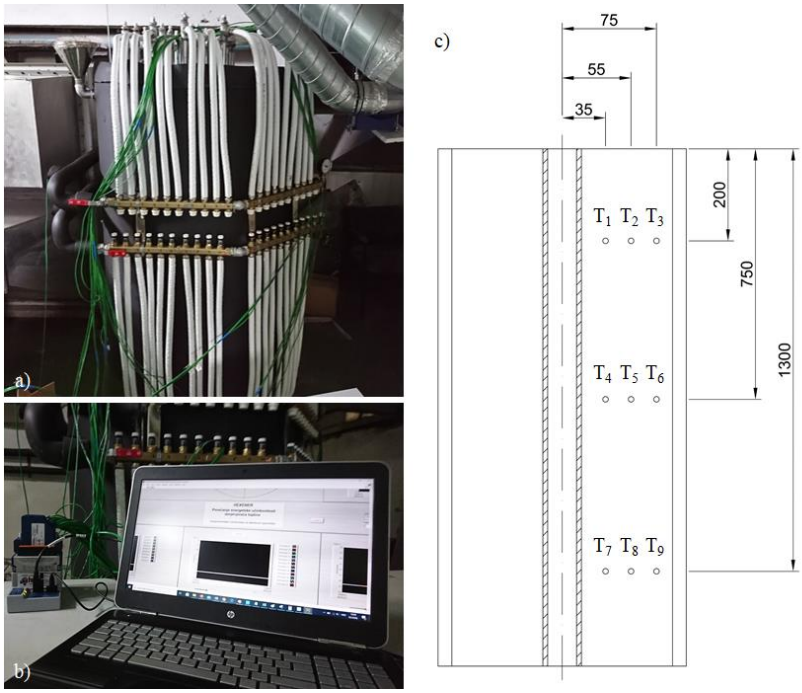

Fig. 3. Experimental setup, a) experimental LTES tank, b) data acquisition set and personal computer, c) thermocouples position and nomenclature

Experimental measurements were performed during the PCM melting and solidification processes for a variety of operating conditions. Validation was performed by comparing the PCM transient temperature variations obtained numerically with those obtained experimentally during both melting and solidification processes. In Fig. 4, a comparison of transient PCM temperature variations obtained experimentally and numerically during both melting and solidification processes at position T_3 is shown.

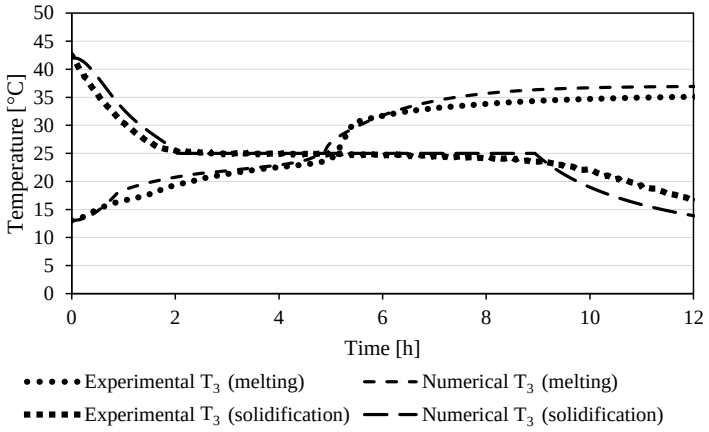

Fig. 4. Comparison of transient temperature variations during melting and solidification obtained experimentally and numerically at position T_3

The comparison was performed with the total HTF mass flow rate of 0.185 kg/s, which corresponds to an inlet velocity of 0.02 m/s through each tube. For the melting process, the HTF inlet temperature was 37 °C, while for the solidification process, the HTF inlet temperature was 10 °C. Initial temperatures of the PCM were uniform throughout the domain at the start of both melting and solidification experiments and were 13 °C and 42 °C, respectively. As evident from Fig. 4, good agreement between experimental and numerical results was observed for both melting and solidification processes. Additional comparisons, featuring different axial and radial positions and discussion of relative errors between experimental and numerical results, can be found in Kirincic et al. (2021b).

4. Numerical results and discussion

Influence of fin thickness (δ) on heat transfer during PCM melting and solidification processes has been numerically investigated by comparing thermal performances of three LTES configurations with different fin thicknesses; 0.5 mm, 2 mm and 4 mm. The numerical investigation has been performed with the HTF inlet velocity ($w_{HTF,in}$) of 0.02 m/s in both melting and solidification investigations. HTF inlet temperature ($T_{HTF,in}$) was 42 °C in melting investigations and 7 °C in solidification investigations. Initial temperature ($T_{PCM,init}$) was homogenous throughout the domain; 13 °C in melting investigations and 42 °C in solidification investigations. Since there is a slightly larger initial temperature difference between the HTF in the PCM in solidification investigations compared to melting investigations, LTES discharging capacity is approximately 5% larger as a result.

Thermal performances of LTES with different fin thicknesses have been assessed by comparing melting and solidification rates, through temperature and liquid fraction distributions, transient average liquid fraction variations and transient variations of average fin temperatures, as well as stored and released thermal energies in selected charging and discharging times for the PCM annulus surrounding a single HTF tube.

For investigated LTES configurations with selected fin thicknesses, temperature and liquid fraction distributions in the xy plane at z = 750 mm have been shown during melting in calculation times of 1, 3 and 5 h (Fig. 5) and during solidification in calculation times 2, 5 and 8 h (Fig. 6), while transient average variations of liquid fraction during melting and solidification have been shown in Fig. 7.

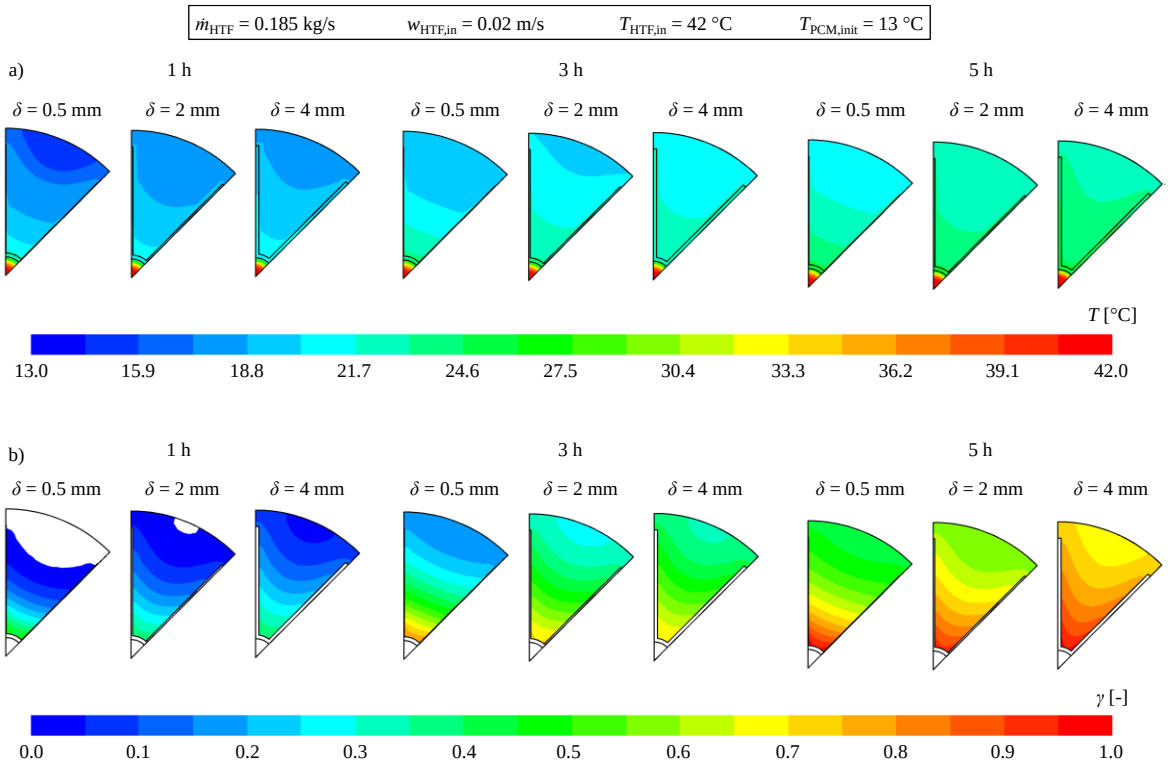

Fig. 5. Temperature (a) and liquid fraction (b) distributions obtained during melting in the xy plane at z = 0.75 m for LTES configurations with fin thicknesses of 0.5 mm, 2 mm and 4 mm

From the comparison of temperature and liquid fraction distributions of LTES configuration with different fin thicknesses in equivalent calculation times, it can be concluded that the most intense heat transfer for both melting and solidification processes is achieved for the largest fin thickness of 4 mm, while the least intense heat transfer is achieved for the smallest fin thickness of 0.5 mm. From liquid fraction distributions, a faster advancement of both the melting and solidification front can be seen in the configuration with the largest considered fin thickness. Similar can be observed from the variations of liquid fraction, from which melting and solidification times can be observed. Melting time for the LTES configurations with 4 mm, 2 mm and 0.5 mm fin thicknesses are 8.67 h, 9.17 h and 11.75 h, respectively, while solidification times for same

configurations are 12.89 h, 14.48 h and 16.64 h, respectively. The investigation also revealed that variations in fin thickness surface area modestly affect heat transfer, as they are increased by 1.5% and decreased by 1.1% in configurations with 4 mm and 0.5 mm compared to the 2 mm fin configurations, respectively. Significant difference in heat transfer is a result of a significantly larger heat capacity of thicker fins, which is directly linked to fin volume and consequently, its mass. For thicker fins, this results in higher average fin temperatures throughout the entire charging process and lower average fin temperatures throughout the discharging process. In order to illustrate that, transient variations of average fin temperatures during charging and discharging have been provided in Fig. 8.

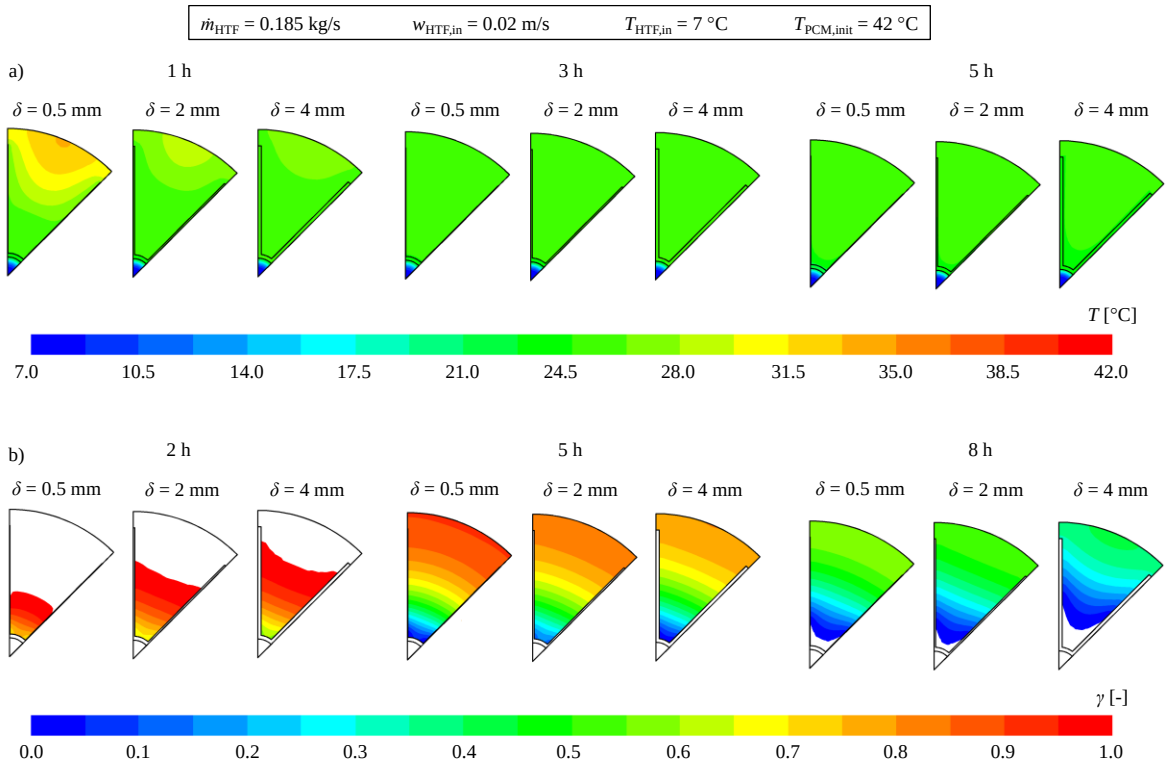

Fig. 6. Temperature (a) and liquid fraction (b) distributions obtained during solidification in the xy plane at z = 0.75 m for LTES configurations with fin thicknesses of 0.5 mm, 2 mm and 4 mm

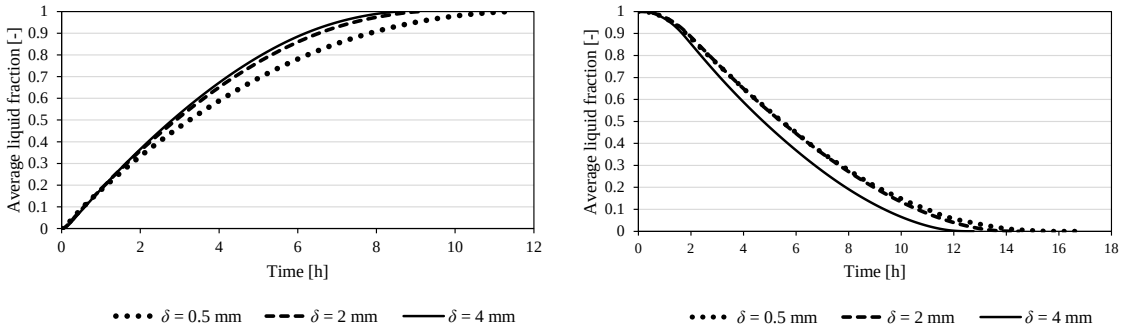

Fig. 7. Comparison of transient average liquid fraction variations during melting (left) and solidification (right) for LTES configurations with fin thicknesses of 0.5 mm, 2 mm and 4 mm

However, increasing fin thickness in a LTES of constant volume also means that the LTES thermal energy storing capacity reduces. For a single LTES tube and its surrounding PCM annulus, values of thermal energy stored in 8 h and released in 12 h have been given in Fig. 9. Stored and released thermal energies are calculated as a sum of sensible and latent thermal energies obtained for the PCM region surrounding the tube. It can be observed that in the 8 h of charging the most thermal energy is stored inside the LTES with 2 mm fin thickness,

6163.3 kJ. Due to lower fin heat capacity resulting in poorer heat transfer, less thermal energy is stored inside the LTES with 0.5 mm fin thickness, 6055.9 kJ. For the LTES with 4 mm fin thickness, 6059.7 kJ is stored in the equivalent charging time. Similarly, in 12 h of discharging, the most thermal energy is also released for the LTES with 2 mm thick fins, 6297.8 kJ, while for LTES configurations with 0.5 mm (6158.7 kJ) and 4 mm thick fins (6291.3 kJ), less thermal energy was released due to lower fin capacity which resulted in lesser heat transfer and reduced amount of the PCM, respectively. Even though thicker fins are beneficial for heat transfer, they decrease the amount of the PCM inside the LTES and result in less stored thermal energy.

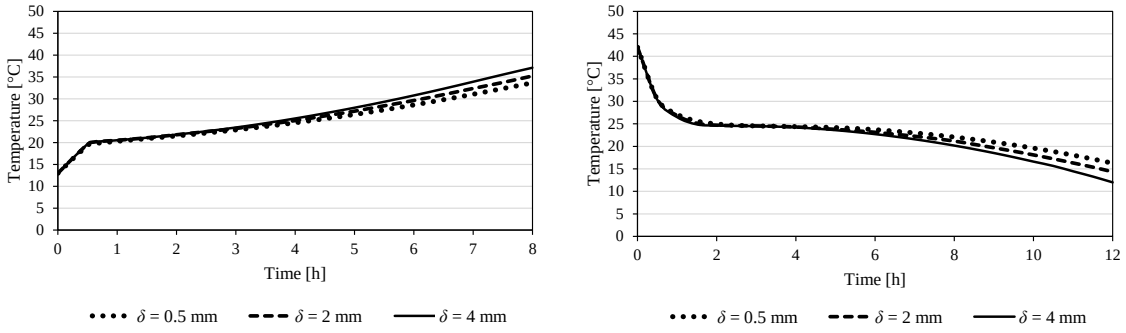

Fig. 8. Comparison of transient average fin temperatures variations during melting (left) and solidification (right) for LTES configurations with fin thicknesses of 0.5 mm, 2 mm and 4 mm

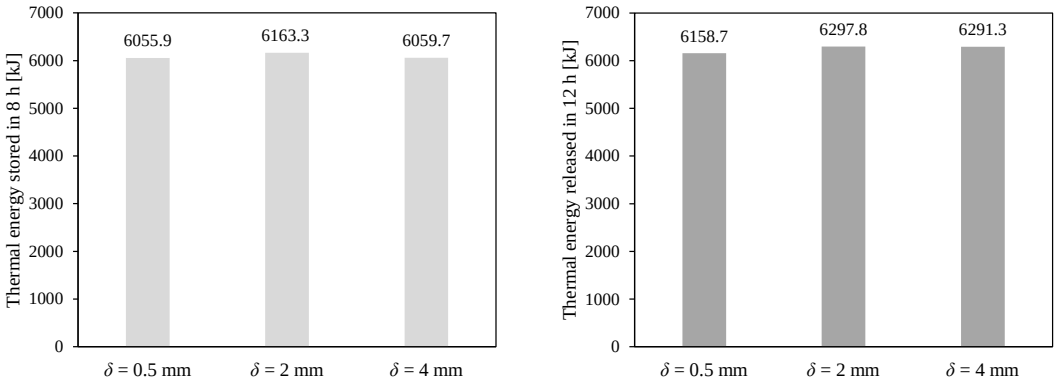

Fig. 9. Comparison of thermal energies stored during 8 h of charging (left) and released during 12 h of discharging (right) for LTES configurations with fin thicknesses of 0.5 mm, 2 mm and 4 mm

5. Conclusion

The paper presented the results of the numerical investigation of the influence of fin thickness on longitudinally finned LTES melting and solidification thermal performance. LTES configurations with fin thicknesses of 0.5 mm, 2 mm and 4 mm were investigated and it was observed from temperature and liquid fraction distributions, transient variations of average liquid fraction and average fin temperatures that thicker fins considerably expedite melting/solidification rate. However, thicker fins also reduce the amount of the PCM inside the LTES, which can result in reduced LTES thermal energy storing/releasing capacity. As observed from obtained stored/released thermal energies for analyzed fin thicknesses, the largest amount of thermal energy was stored/released for the configuration with 2 mm fin thickness. Based on the investigation, it is evident that fin thickness is an influential geometry parameter which needs to be selected carefully in order to enhance the LTES thermal performance.

6. Acknowledgments

This work has been supported in part by Croatian Science Foundation under the project HEXENER (IP-2016-06-4095) and in part by the University of Rijeka under the project numbers “uniri-iskusni-tehnic-23-180” and “uniri-mladi-tehnic-23-8”.

7. References

Brent, A.D., Voller, V.R., Reid, K.J., 1988. Enthalpy-porosity technique for modeling convection-diffusion phase change: application to the melting of a pure metal, Numerical Heat Transfer, 13 (3), 297–318.

Fteiti, M.A., Ghalambaz, M., Younis, O., Sheremet, M., Ismael, M., 2023. The influence of the metal foam layer shape on the thermal charging response time of a latent heat thermal energy storage system, Journal of Energy Storage, 58, 106284.

Khan, Z., Khan, Z., Ghafoor, A.., 2016. A review of performance enhancement of PCM based latent heat storage system within the context of materials, thermal stability and compatibility, Energy Conversion and Management, 115, 132–158.

Khan, Z., Khan, Z.A., 2017. Experimental investigations of charging/melting cycles of paraffin in a novel shell and tube with longitudinal fins based heat storage design solution for domestic and industrial applications, Applied Energy, 206, 1158–1168.

Kirincic, M., 2021. Experimental and numerical analysis of the latent thermal energy storage performance enhancement, PhD thesis, University of Rijeka, Faculty of Engineering, Rijeka, Croatia, (in Croatian).

Kirincic, M., Trp, A.., Lenic, K., 2021. Numerical evaluation of the latent heat thermal energy storage performance enhancement by installing longitudinal fins, Journal of Energy Storage, 42, 103085.

Kirincic, M., Trp, A., Lenic, K., 2021. Influence of natural convection during melting and solidification of paraffin in a longitudinally finned shell-and-tube latent thermal energy storage on the applicability of developed numerical models, Renewable Energy, 179, 1329–1344.

Kirincic, M., Trp, A., Lenic, K., Wolf, I., 2021. Experimental investigation on melting of paraffin in latent thermal energy storage, Proceedings of the 14th International Renewable Energy Storage Conference 2020 (IRES 2020), 193–198.

Kirincic, M., Trp, A., Lenic, K., Torbarina, F., 2024. Numerical analysis of the influence of geometry parameters on charging and discharging performance of shell-and-tube latent thermal energy storage with longitudinal fins, Applied Thermal Engineering, 236 (A), 121385.

Kirincic, M., Trp, A., Lenic, K., Batista, J., 2024. Latent thermal energy storage performance enhancement through optimization of geometry parameters, Applied Energy, 365, 123255.

Kumar, A., Saha, S.K., 2020. Experimental and numerical study of latent heat thermal energy storage with high porosity metal matrix under intermittent heat loads, Applied Energy, 263, 114649.

Liu, M., Saman, W., Bruno, F., 2012. Review on storage materials and thermal performance enhancement techniques for high temperature phase change thermal storage systems, Renewable and Sustainable Energy Reviews, 16, 2118–2132.

Modi, N., Wang, X., Negnevitsky, M., 2023. Numerical investigation into selecting the most suitable shell-to-tube diameter ratio for horizontal latent heat thermal energy storage, Energy for Sustainable Development, vol. 73, 188–204.

Rathod, M.K., Banerjee, J., 2015. Thermal performance enhancement of shell and tube Latent Heat Storage Unit using longitudinal fins, Applied Thermal Engineering, 75, 1084–1092.

Versteeg, H.K., Malalasekera, W., 1995. An Introduction to Computational Fluid Dynamics: The Finite Volume Method, Longman Scientific and Technical, Essex, England.

Yang, X., Lu, Z., Bai, Q., Zhang, Q., Jin, L., Yan, J., 2017. Thermal performance of a shell-and-tube latent heat thermal energy storage unit: Role of annular fins, Applied Energy, 202, 558–570.

Yu, C., Zhang, X., Chen, X., Zhang, C., Chen, Y., 2020. Melting performance enhancement of a latent heat storage unit using gradient fins, International Journal of Heat and Mass Transfer, 150, 119330.

Yu, D., Qiu, Y., Zhang, X., 2023. Role of nano-copper in discharging performance of latent heat storage unit, International Communications in Heat and Mass Transfer, 144, 106748.

RT 25 data sheet, Rubitherm GmbH, 2018.

List of symbols

A_{mush}	morphological constant (kg/m^{3}s)
c	specific heat capacity (J/kgK)
g	gravitational acceleration (m/s^2)
H	specific enthalpy (J/kg)
k	thermal conductivity (W/mK)
L	specific latent heat (J/kg)
$\dot{m}$	mass flow rate (kg/s)
p	pressure (Pa)
p^*	pressure reduced by hydrostatic component (Pa)
S	source term in momentum equations (N/m^3)
T	temperature (K)
t	time (s)
w	velocity (m/s)
x, y, z	spatial coordinates (m)
β	thermal expansion coefficient (1/K)
γ	liquid fraction (-)
δ	fin thickness (m)
ε	numerical constant (-)
μ	dynamic viscosity (Pa·s)
ρ	density (kg/m^3)

Subscripts

0	reference
HTF	heat transfer fluid
in	inlet
init	initial
l	liquidus
n	normal
PCM	phase change material
s	solidus
w	wall
x, y, z	spatial coordinates